Supporting Information

Strain-correlated Piezoelectricity in Quasi-two-dimensional Zinc-oxide Nanosheets

Corey Carlos[1], Jun Li[1], Ziyi Zhang[1], Kevin Jordan Berg[1], Yizhan Wang[1], Xudong Wang[1,*]

[1]*Department of Materials Science and Engineering, University of Wisconsin–Madison, Madison, Wisconsin 53706, United States*

**Corresponding Author: Xudong Wang, Email: xudong.wang@wisc.edu*

Methods

3D Printed AFM Mounts. Application of uniaxial compressive and tensile strain was achieved via a series of eight 3D printed AFM mounts (4-concave, 4-convex), where concave mounts correspond to the compressive configuration and vice versa. Printing of the 3D mounts was accomplished by an Anycubic DLP 3D printer using a commercial resin available from Anycubic. The radius of curvature (ROC) for these mounts, in order of increasing strain, was: [1] 20 mm, [2] 17.5 mm, [3] 15 mm, and [4] 12.5 mm, where the 4-convex and 4-concave mounts each had a matching ROC for its opposite strain configuration (i.e., 20 mm convex → 20 mm concave).

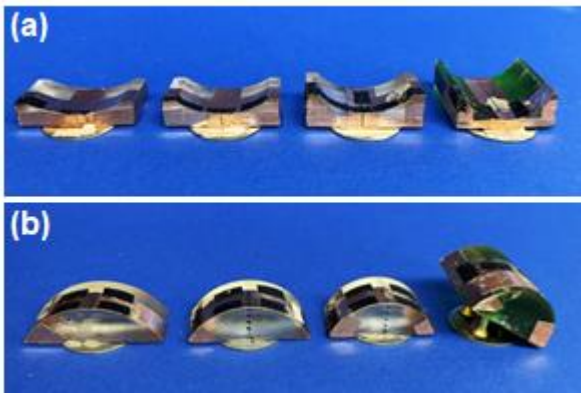

Figure S1. 3D printed (a) concave and (b) convex mounts used to enable strain-correlated PFM measurements.

Sample Preparation. Synthesis of 2D ZnO-NSs (see Figure S2) was accomplished using a liquid-air interfacial growth technique known as ionic layer epitaxy (ILE), where the details of this technique have been explored broadly in our previous work. To achieve air/water interfacial growth, a metal-salt precursor solution was prepared using a 50 mL deionized water 25 mM $Zn(NO_3)_2$:hexamethylenetetramine solution, which was then transferred evenly between three 24 mL vials. An 8 µL drop of chloroform solution containing 1.8 mM sodium oleyl sulfate (SOS): oleyl-amine (OAM) [9:1] was then dispersed at the air/water interface of each vial and each solution system was left to rest at room temperature for 10-minutes. The 24 mL vials were then

sealed and placed into a convection oven at 60 °C for 35-minutes. A Ti/Au-coated polyimide (PI) substrate with a thickness of 0.125 mm served as a flexible supporting substrate, as well as the bottom conducting electrode for the strain correlated PFM measurements. The Ti/Au-coated [5nm/45nm] PI was prepared via metal evaporation/deposition using an E-beam Evaporator (CHA-600) at a deposition rate of 0.03 nm/s and 0.05 nm/s, respectively. Preparation of the ZnO-NSs used in the normal loading force experiments (see Figure S3) was similar to the strained-correlated ZnO-NSs, except a rigid Si/Ti/Au-coated [3nm/17nm] substrate served as a support and bottom electrode surface. Upon completion of the ILE reaction, the three vials were removed from the convection oven and a Ti/Au-coated PI substrate (or rigid Au/Ti/Si substrate) was used to scoop the ZnO-NSs at the air/water interface.

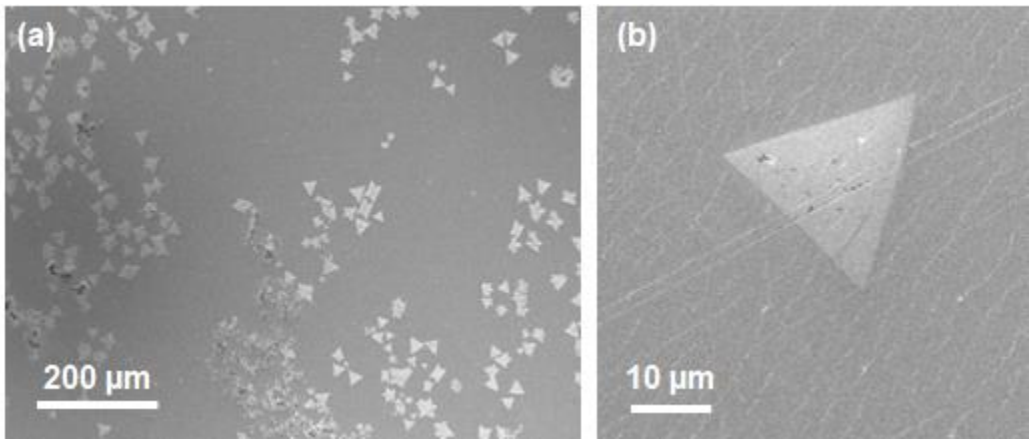

Figure S2. Scanning electron microscopy images show (a) distribution of 2D ZnO-NSs and (b) strong morphology of the [0001] ZnO-NS examined in the strain correlated PFM measurements.

Section 1 (S1): Piezoelectric characterization

PFM measurements were performed using the dynamic contact electrostatic force microscopy (DC-EFM) mode on a Park Systems XE-70 multimode atomic force microscope (AFM) in the contact regime. To separate the small signal amplitude and phase response associated with the converse piezoelectric effect of the ZnO-NS, a lock-in amplifier (LiA) technique was employed using a Stanford Research 830 (SR830). A MikroMasch NSC14/Cr-Au cantilever with a tip radius of < 30.0 nm and a nominal force constant of 5.0 N/m was chosen for the strained correlated PFM measurements.

A set of loading force experiments were conducted to show the piezoelectric response under increased normal loading and to mitigate tip electrostatics (TES) by the AFM probe. From the normal loading force (⊥F) experiments in Figure S3c, we showed that the piezoelectric response saturates for normal loads > 40 nN, which we argue minimizes the TES forces and better resolves the pure piezoresponse from the ZnO-NS. Therefore, a set point of 50 nN (⊥F) was chosen for conducting the strain-correlated PFM measurements.

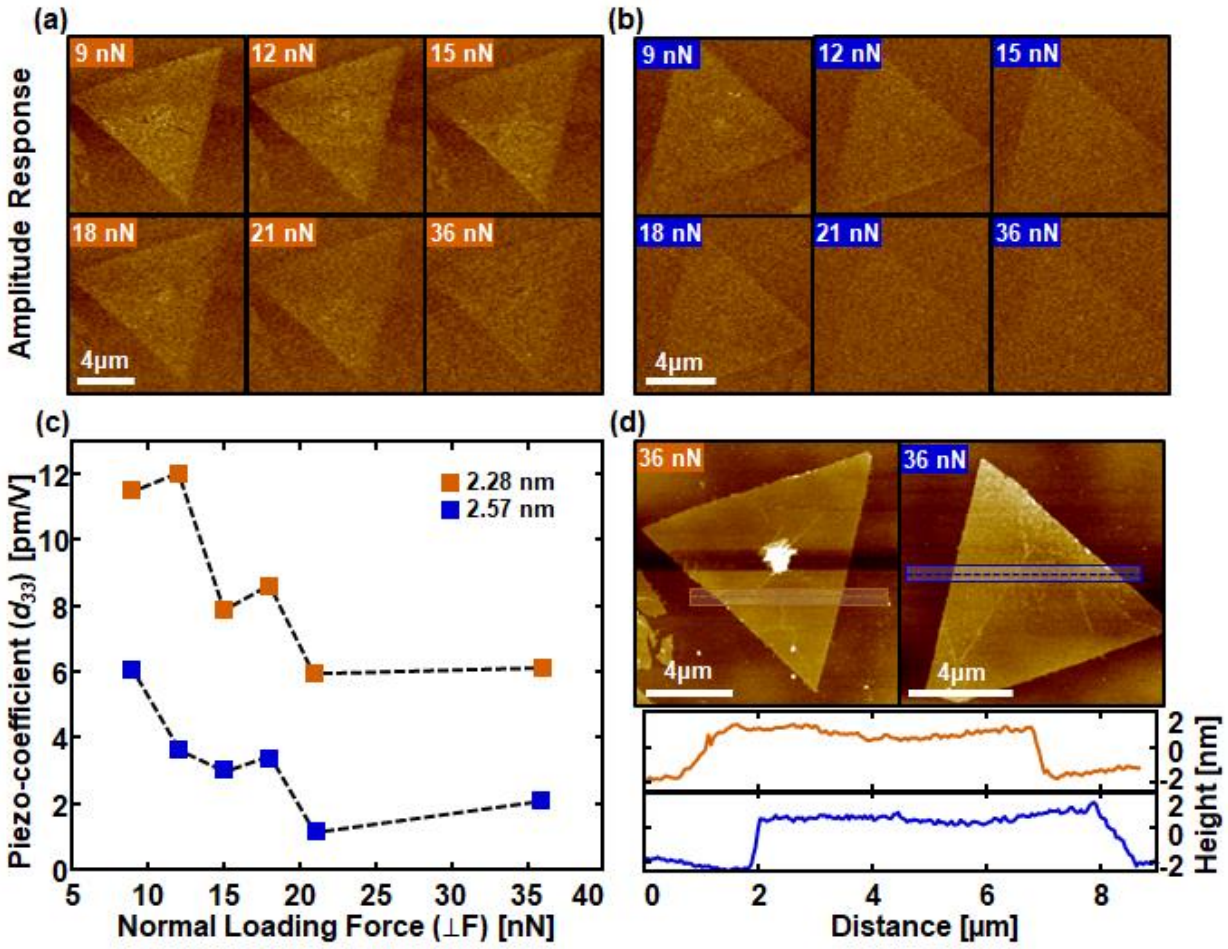

Figure S3. PFM measurements taken on rigid Au-coated Si show (a/b) the amplitude response of 2D ZnO-NSs and (c) extracted piezoelectric coefficient, or d_{33}, shows a strong saturation for increased normal loading of the AFM cantilever-tip. For ZnO-NSs synthesized using the ILE method, the (d) thicknesses can routinely be tailored to ~2.4 nm with good morphology typical of wurtzite ZnO.

Finally, the surface roughness was extracted for both rigid Au-coated silicon (Si) and flexible Au-coated polyimide (PI) substrates shown in Figure S3. Given the larger surface roughness (~3.4 nm) when compared to the thickness of the ZnO-NS (t ~ 2.4 nm), Figure S4b illustrates the challenges associated with PFM imaging on the flexible PI, which necessitates a coupled lateral force microscopy/PFM technique. It is noted that the regions selected for quantifying surface roughness on the PI were "smooth", however, the larger scratches/imperfections would indeed increase extracted values in Table S1. The LFM inset in Figure S4b shows how one could resolve sample location and morphology using such an LFM/PFM method.

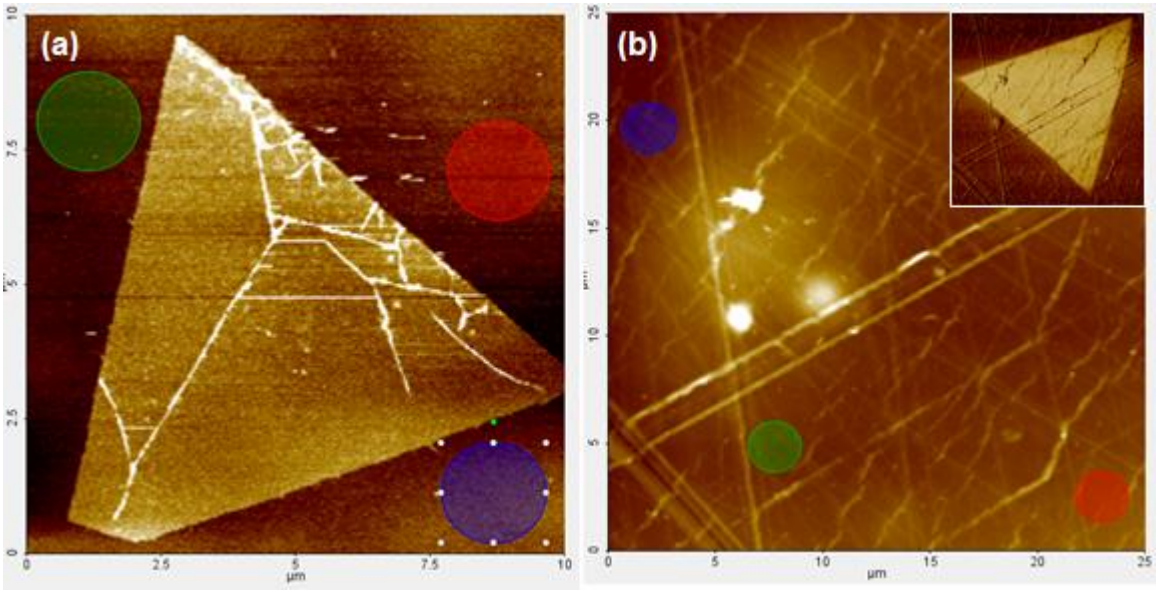

Figure S4. Selected regions used to determine the surface roughness of (a) rigid Au-coated Si and (b) flexible Au-coated PI substrates, inset shows lateral force microscopy image of measured ZnO-NS.

Table S1. Measured surface roughness of supporting substrates.

Substrate	Red	Green	Blue	Average Surface Roughness (nm)
Rigid Au-Coated Silicon (Si)	0.364	0.405	0.439	0.403
Flexible Au-coated Polyimide (PI)	3.336	2.815	4.172	3.441

Section 2 (S2): Experimental parameters

Several efforts were made to minimize and quantify sources of error during the strained-correlated PFM study (see Figure S5). First, upon transferring the ZnO-NS/PI-substrate onto the 3D printed mount, grounding to the conductive AFM disk is achieved via Ag-paste such that an electric field can be generated between the conductive AFM cantilever-tip and Au-coated PI substrate. The Ag-paste grounding was monitored via multimeter by measuring the resistance from the PI substrate to the AFM disk, with an average grounding of 5.86 Ω (± 2.11 Ω); more than sufficient for strong electric field generation at the tip-sample junction. Next, we calibrated the vertical sensitivity (Z) V-μm^{-1} of the cantilever tip by taking a force vs. displacement curve (Sader Method) on a hard quartz substrate prior to each PFM measurement. The extracted slopes of each curve are shown in S5 by the blue diamonds. Continuous calibration of the AFM cantilever was determined to be critical for monitoring and minimizing small thermal drift in the reflected laser spot from the reflective backside coating of the cantilever. The average vertical sensitivity (Z_{Avg}) was found to be 93.2 V/μm ± 1.36 V/μm, with a variability of ~1.5%. Here the averaged optical lever sensitivity (1/ Z_{Avg}) was found to be ~10.7 ± 0.2 nm/V.

The offset scans are necessary for accurate determination of the out-of-plane piezoelectric response. We recognize that both large (25 × 25 μm^2) and small (1.5 × 1.5 μm^2) offset scans are taken upon the completion of the last small scan PFM measurement (region 4), at 500 μm above the sample surface. Quantifying the out-of-plane piezoelectric response requires measurement of the system noise and oscillating AFM probe behavior in free space, which is captured in the PFM offset scan. By capturing offset scan images, we could use the measured amplitude intensities of the offset scans to remove background noise in the PFM amplitude scans on ZnO-NSs, which was not filtered by the LiA technique. The amplitude intensities of the large

and small scan area offset scans are shown extracted mean intensity values (squares) in S5. From all 18 offset scans, variability was quantified to be ~1.9% with a mean amplitude of 10.3 ± 0.2 mV as read by the AFM's position sensitive photodiode (PSPD).

In addition, to mitigate influence from cantilever-tip degradation and/or ZnO-NS fatigue, the order of the strain correlated PFM measurements were modulated asymmetrically about ε ~ 0.0% configuration. The order of the measurements was as follows: [1] beginning with the largest compressive strain (C4 → ε ~ -0.5%) to the lowest (C1 → ε ~ -0.31%), each strain configuration began with a large scan image followed by the four selected small scan regions, [2] next, the largest tensile strain (T4 → ε ~ +0.50%) to the lowest (T1 → ε ~ +0.31%), [3] finally, the flat (i.e. no strain, ε ~ 0.0%) large scan PFM image was acquired, followed by the four small scan images in the unstrained configuration.

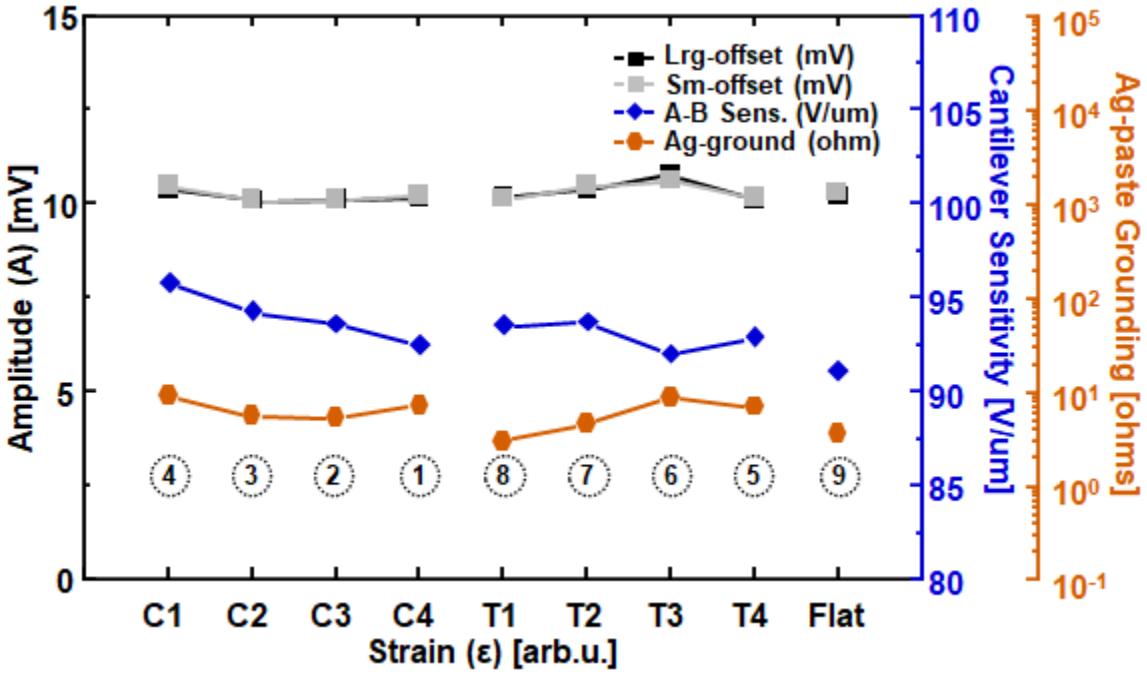

Figure S5. Experimental parameters for the strain correlated PFM measurements. The bottom row of numbers in "dashed circles" show the order in which experiments were performed. The second row of hexagons illustrates the measured grounding of the Ag-paste to the conductive AFM sample disk, where the third row of diamonds quantifies the change in cantilever sensitivity between each experiment. Finally, the top row of overlapping squares indicates the mean intensity values obtained from both large and small amplitude offset scans.

Section 3 (S3): Image Analysis

Using small scan areas solely on the ZnO-NS was critical to minimize the substrate contribution and accurately derive the strain-correlated piezoelectric coefficient. The substrate effects could be influenced by the Young's modulus mismatch between sample/substrate, and is manifested by elevated intensities of subsequent ZnO-NS and substrate amplitude response in the final PFM image sets. This substrate effect became most prominent for the large scan amplitude response at $|\varepsilon\%|$ ~0.42% in the compressive regime (Figure S10), where significant overlap of the substrate (purple curves) and ZnO-NS amplitude intensities (black curves with blue curve fitting) led to a measured d_{33} of ~48.2 pm/V (see Supplemental Figures S9 – 17). When compared to the measured d_{33} for the small scan areas at the same strain (Figure 4b) configuration, we obtained a piezoelectric coefficient of ~20.3 $\pm$2.3 pm/V, for a difference of ~28 pm/V. We note that theoretical work has shown the value of the d_{33} could be enhanced in nanoscale ZnO by surface atom restructuring, where the volume density of surface atoms dominates, resulting in a larger polarization per unit volume. Yet to our best knowledge, no reported experimental research has approached the size regime (< 1 nm) required to achieve enhanced piezoelectricity in ZnO.

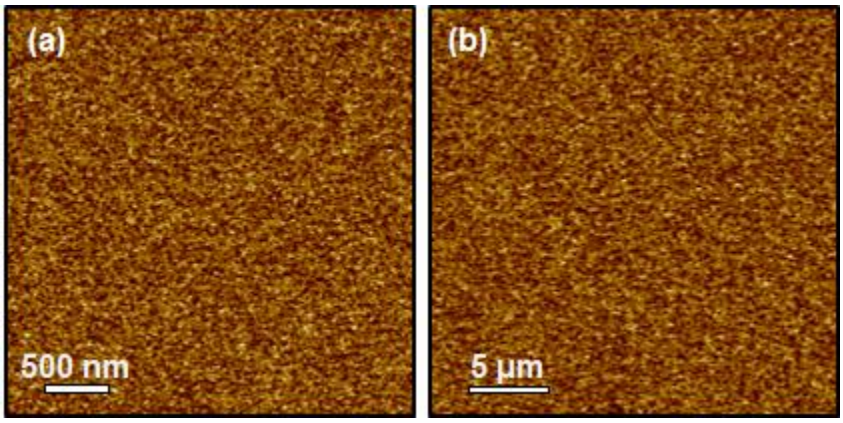

Figure S6. Typical PFM Amplitude image of (a) small and (b) large area offset scan taken ~500 µm above the sample surface.

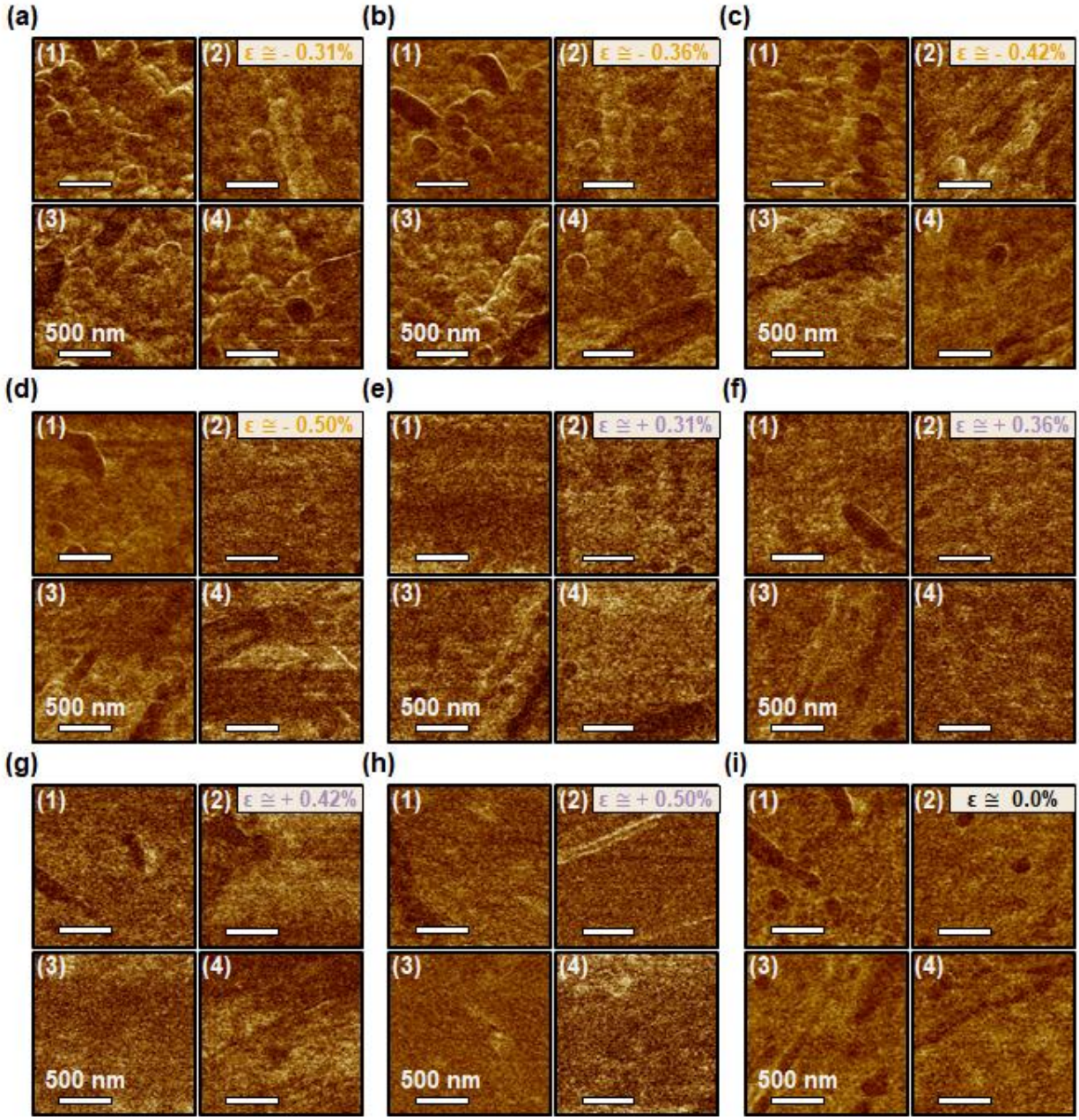

Figure S7. PFM Amplitude images of the four small scan areas (1-4) selected solely on the (0001) ZnO-NS surface. (a-d) Show the small scan area PFM amplitude response on the compressive regime. (e-h) Show the small scan PFM amplitude response of the tensile regime. (i) Small scan area PFM amplitude response of ZnO-NS in unstrained condition.

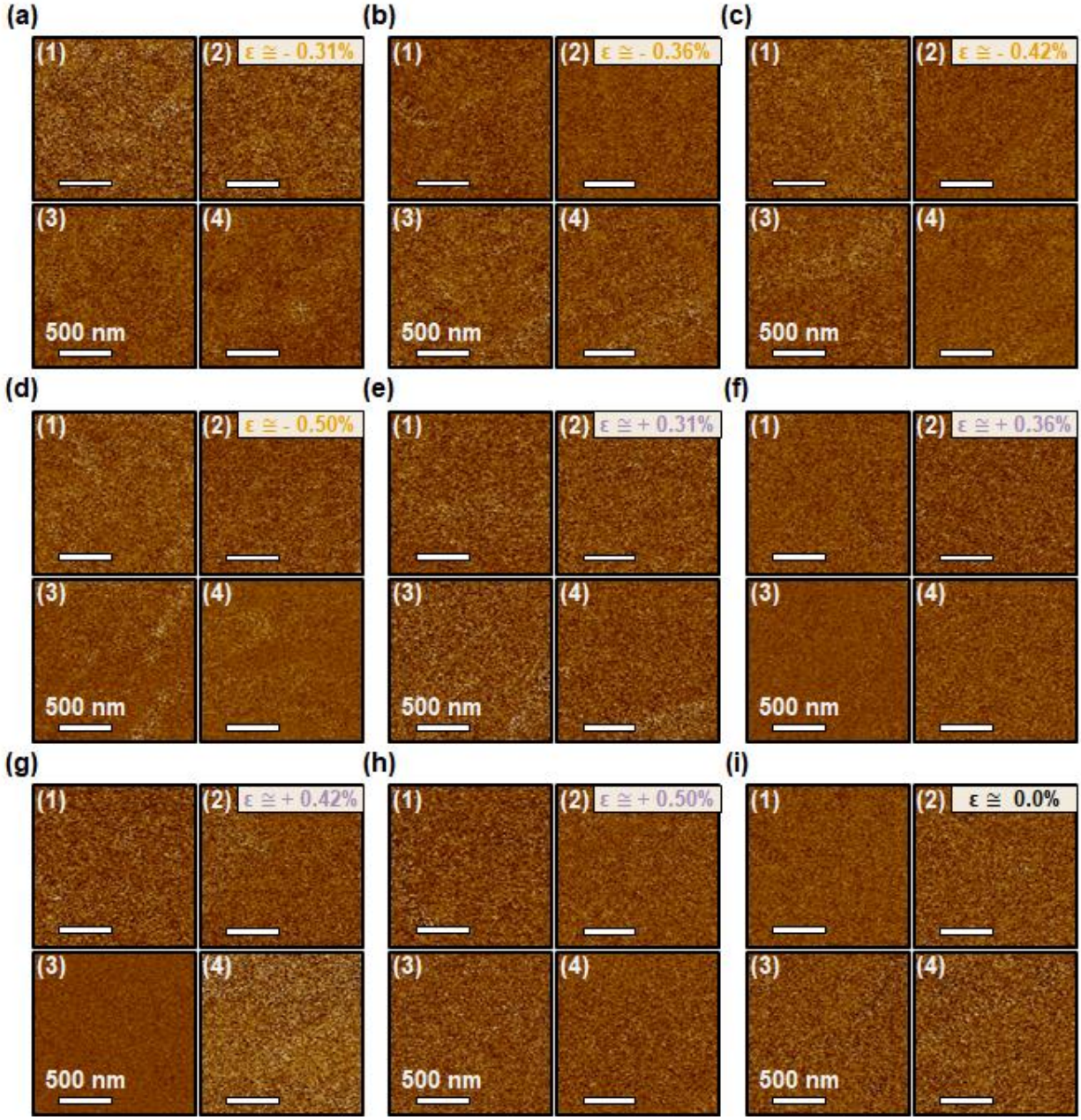

Figure S8. PFM Phase images of the four small scan areas (1-4) selected solely on the (0001) ZnO-NS surface. (a-d) Show the small scan area PFM phase response in the compressive regime. (e-h) Show the small scan PFM phase response of the tensile regime. (i) Small scan area PFM phase response of ZnO-NS in unstrained condition.

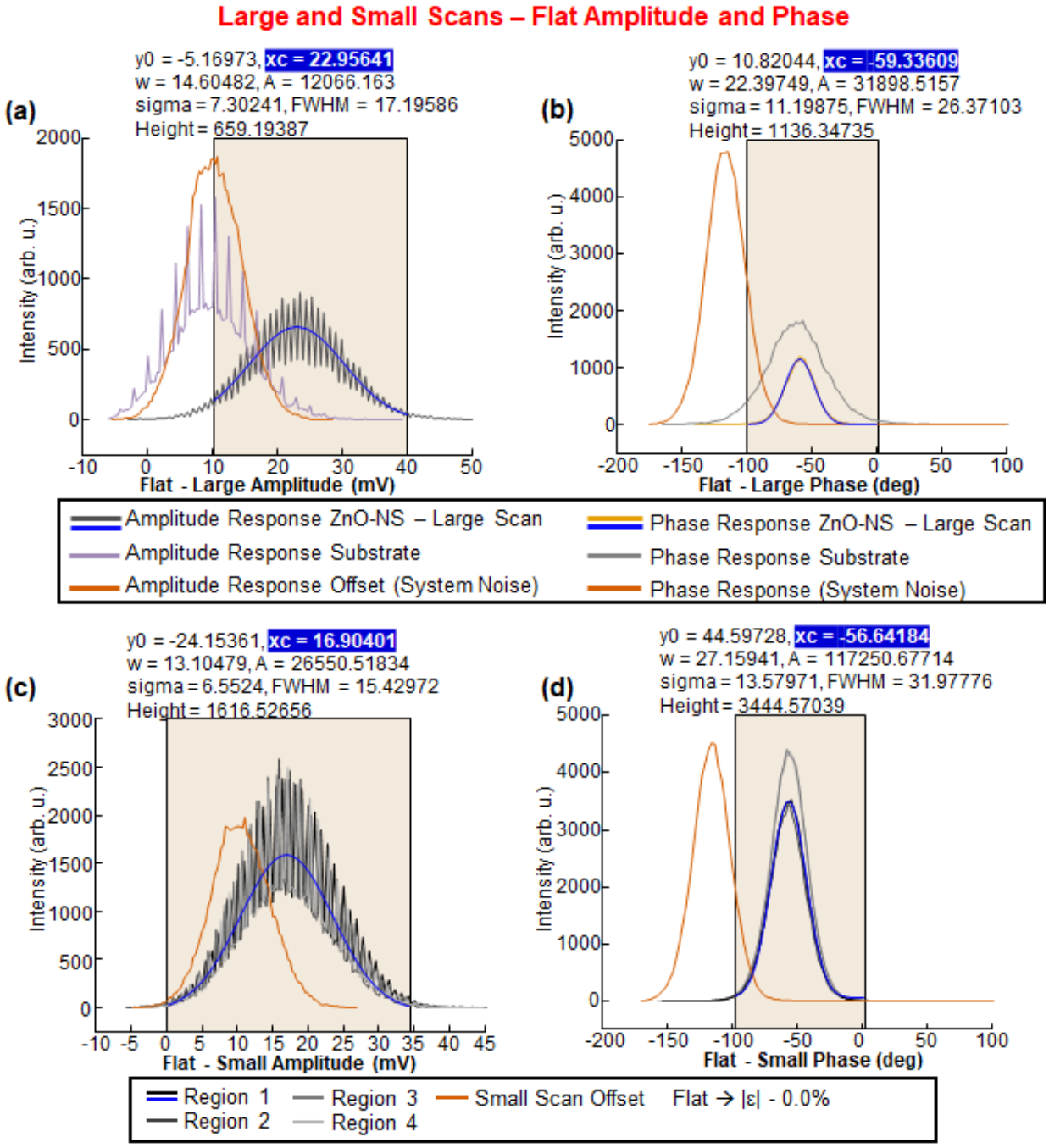

Figure S9. Large scan area (a) Amplitude and (b) Phase image intensity distributions for unstrained configuration. Small scan area (c) Amplitude and (d) Phase image intensity distributions for the four regions selected solely on the ZnO-NS unstrained configuration.

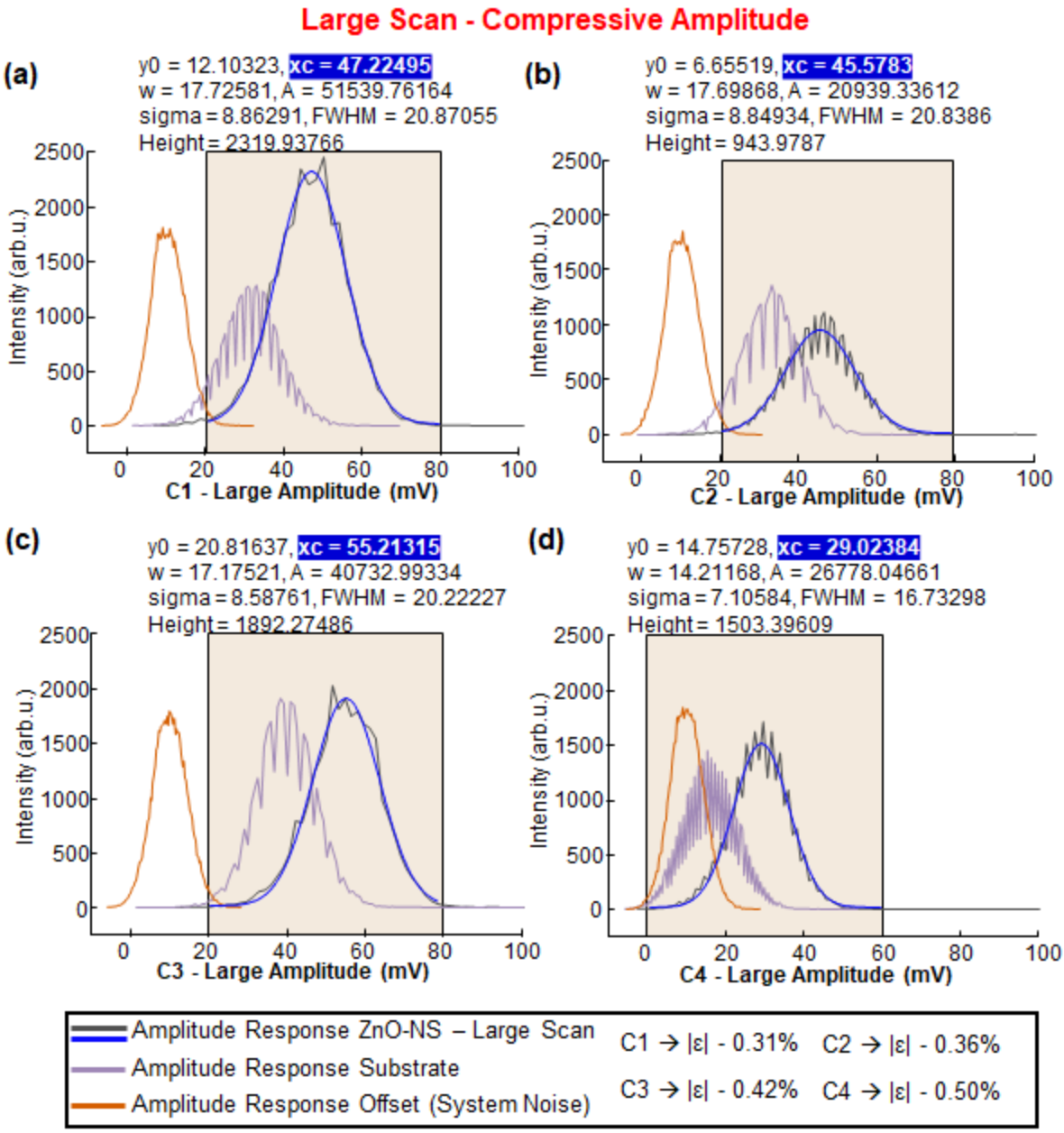

Figure S10. Large scan area PFM Amplitude image intensity distributions for compressive regime at absolute strain of (a) 0.31%, (b) 0.36%, (c) 0.42%, and (d) 0.50%. Extracted means for the ZnO-NS amplitude response highlighted in blue

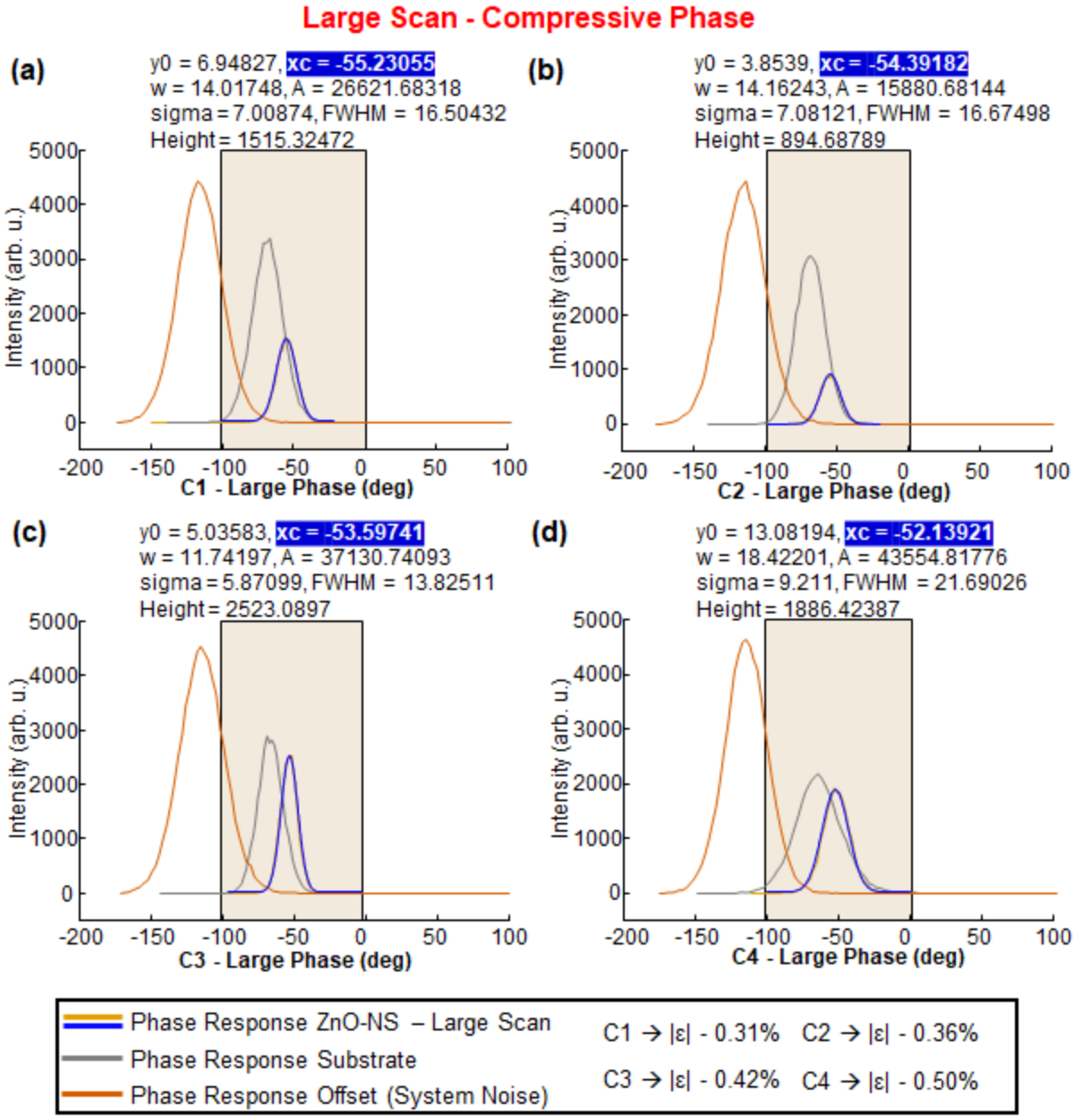

Figure S11. Large scan area PFM Phase image intensity distributions for compressive regime at absolute strain of (a) 0.31%, (b) 0.36%, (c) 0.42%, and (d) 0.50%. Extracted means for the ZnO-NS phase response highlighted in blue.

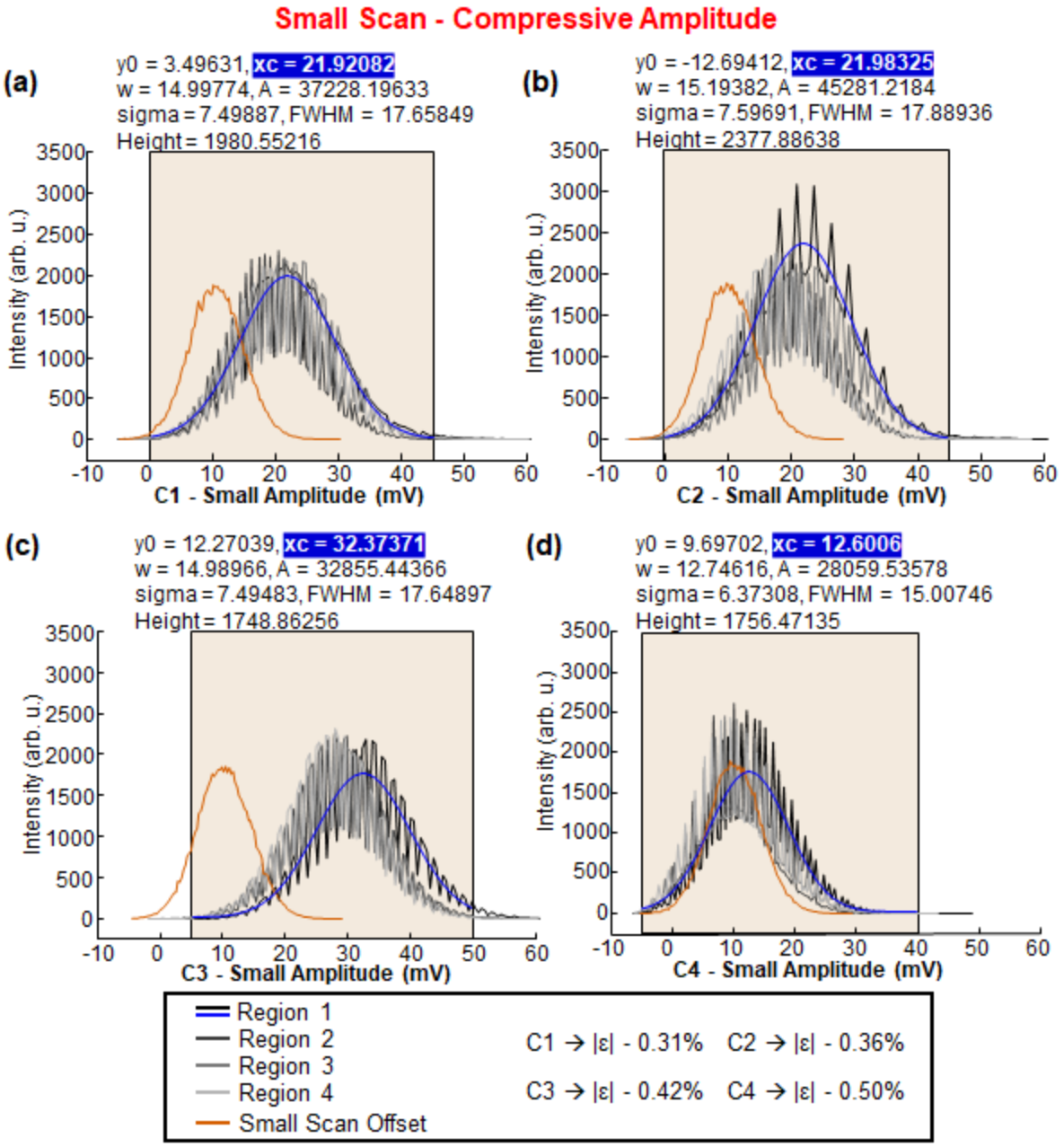

Figure S12. Small scan area PFM Amplitude image intensity distributions of selected regions on ZnO-NS surface for compressive regime at an absolute strain of (a) 0.31%, (b) 0.36%, (c) 0.42%, and (d) 0.50%. Extracted mean for single selected small scan region ZnO-NS amplitude response highlighted in blue.

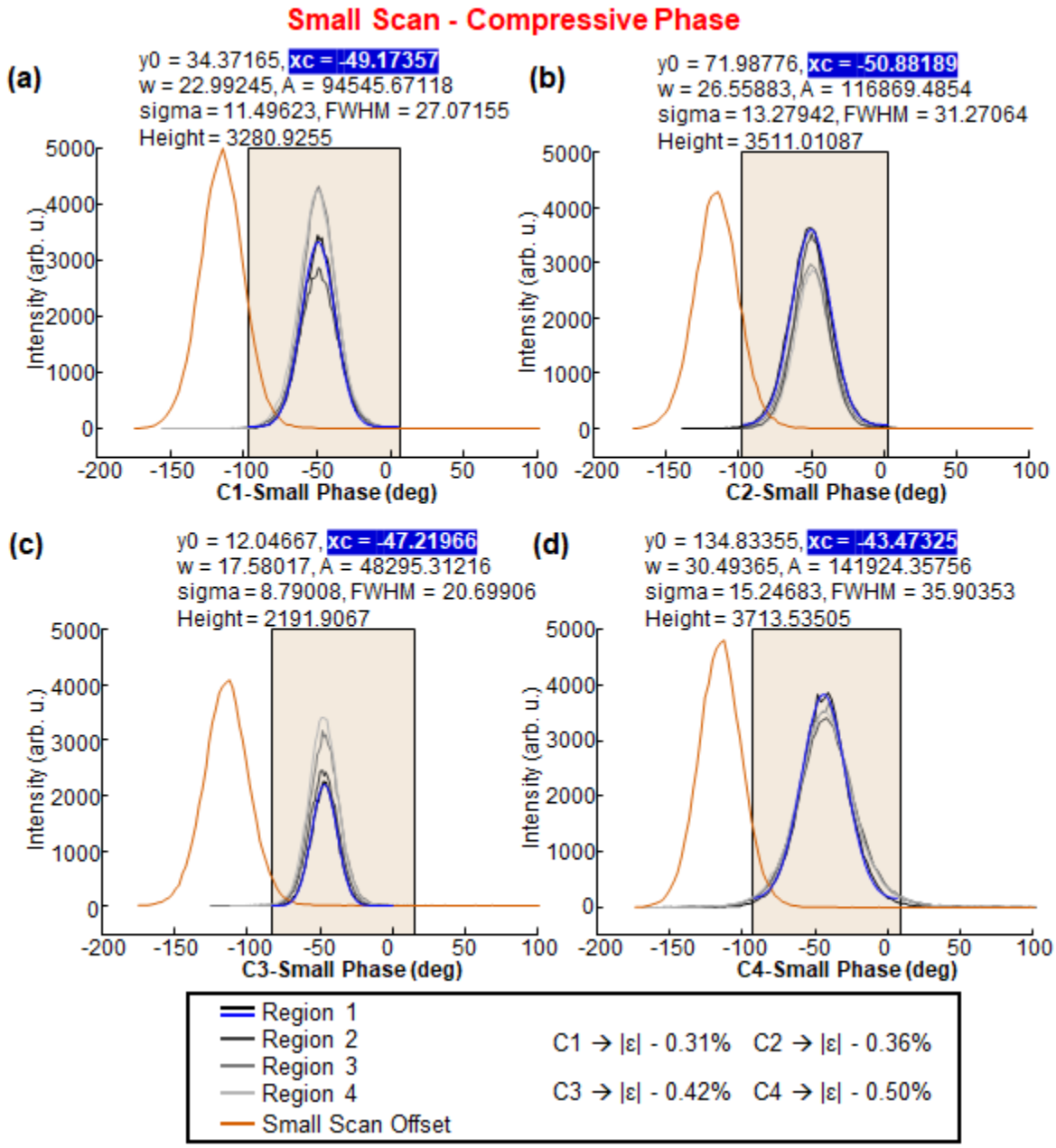

Figure S13. Small scan area PFM Phase image intensity distributions of selected regions on ZnO-NS surface for compressive regime at an absolute strain of (a) 0.31%, (b) 0.36%, (c) 0.42%, and (d) 0.50%. Extracted mean for single selected small scan region ZnO-NS phase response highlighted in blue.

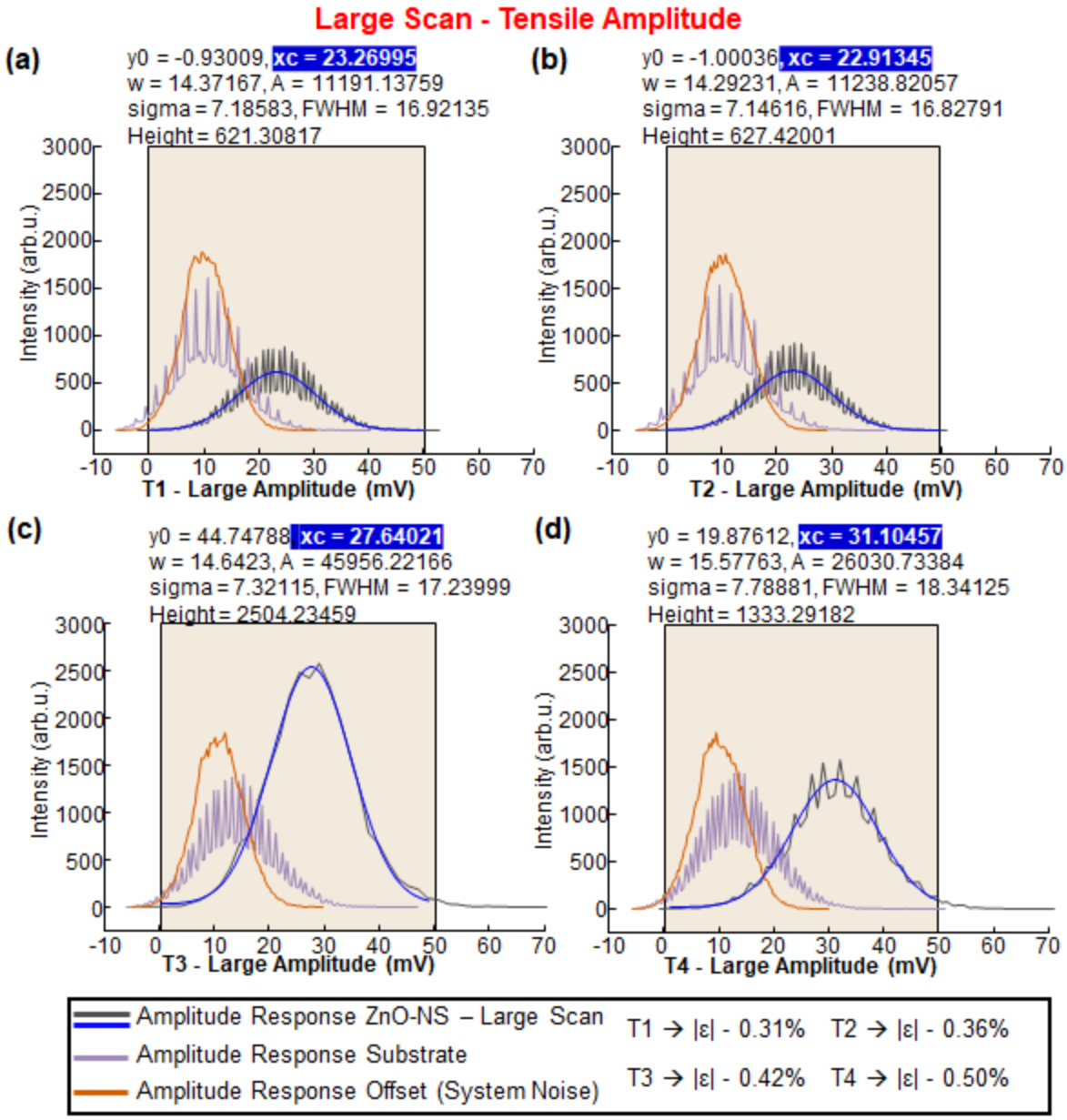

Figure S14. Large scan area PFM Amplitude image intensity distributions for tensile regime at absolute strain of (a) 0.31%, (b) 0.36%, (c) 0.42%, and (d) 0.50%. Extracted means for the ZnO-NS amplitude response highlighted in blue.

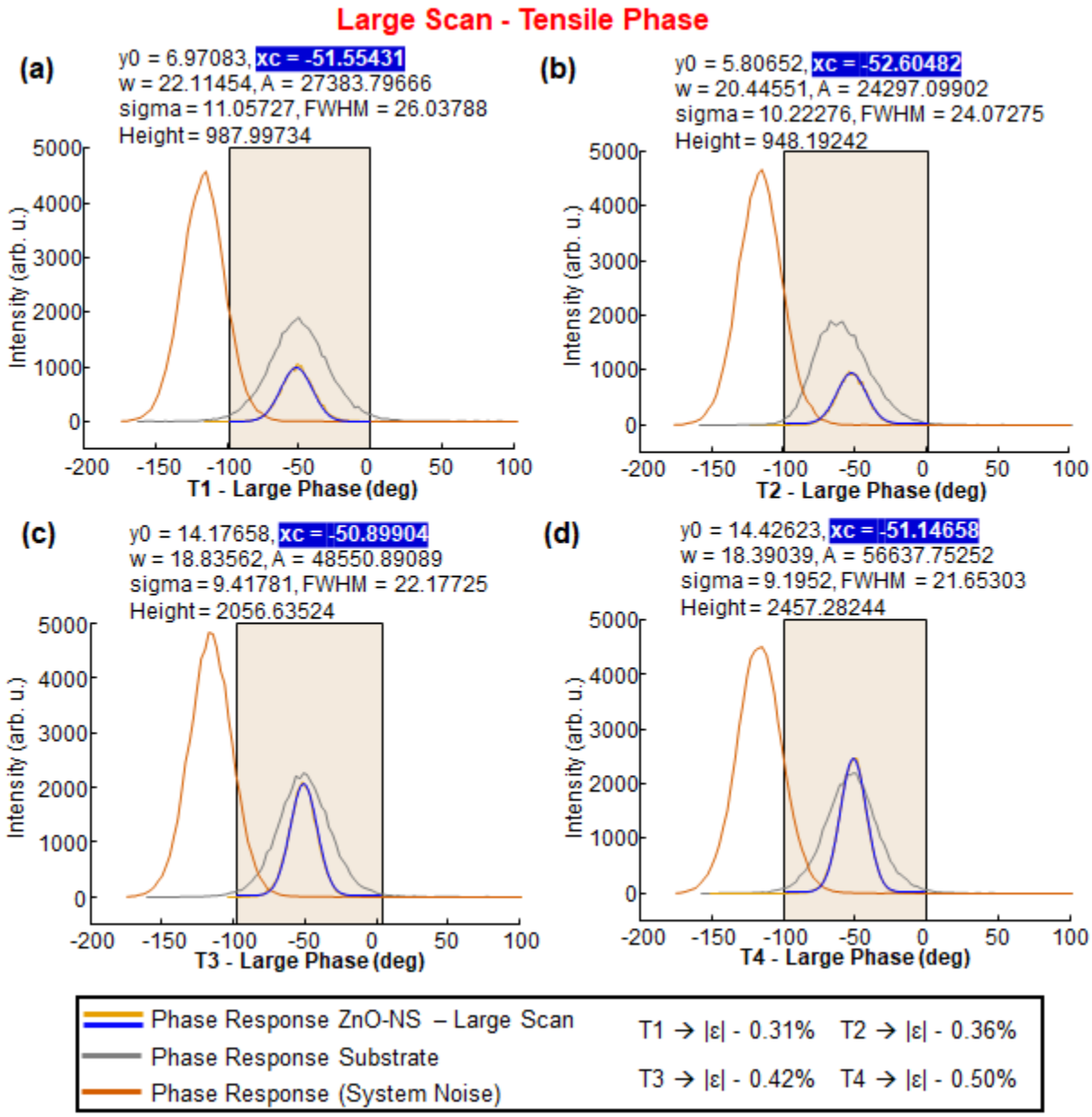

Figure S15. Large scan area PFM Phase image intensity distributions for tensile regime at absolute strain of (a) 0.31%, (b) 0.36%, (c) 0.42%, and (d) 0.50%. Extracted means for the ZnO-NS phase response highlighted in blue.

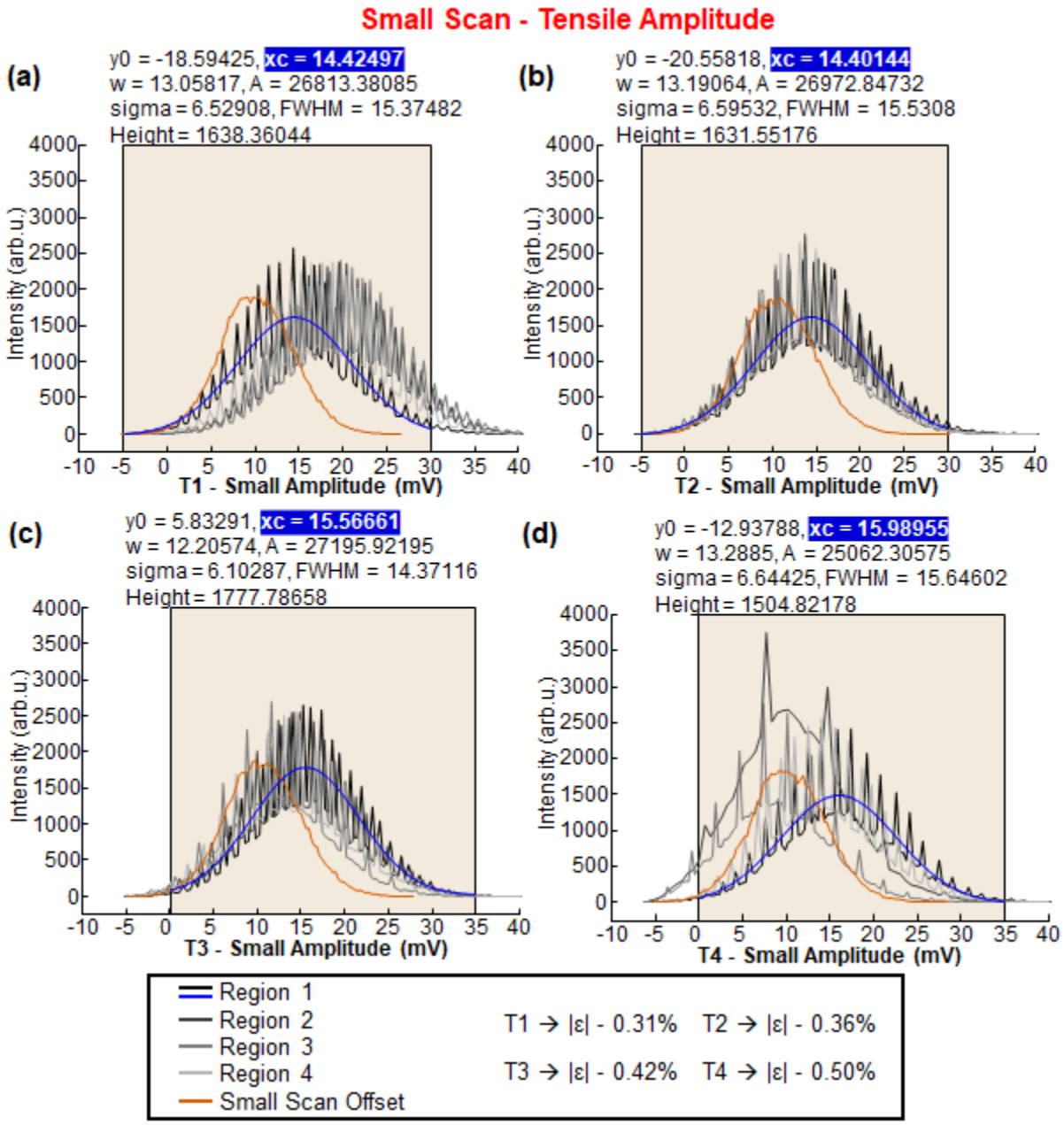

Figure S16. Small scan area PFM Amplitude image intensity distributions of selected regions on ZnO-NS surface for tensile regime at an absolute strain of (a) 0.31%, (b) 0.36%, (c) 0.42%, and (d) 0.50%. Extracted mean for single selected small scan region ZnO-NS amplitude response highlighted in blue.

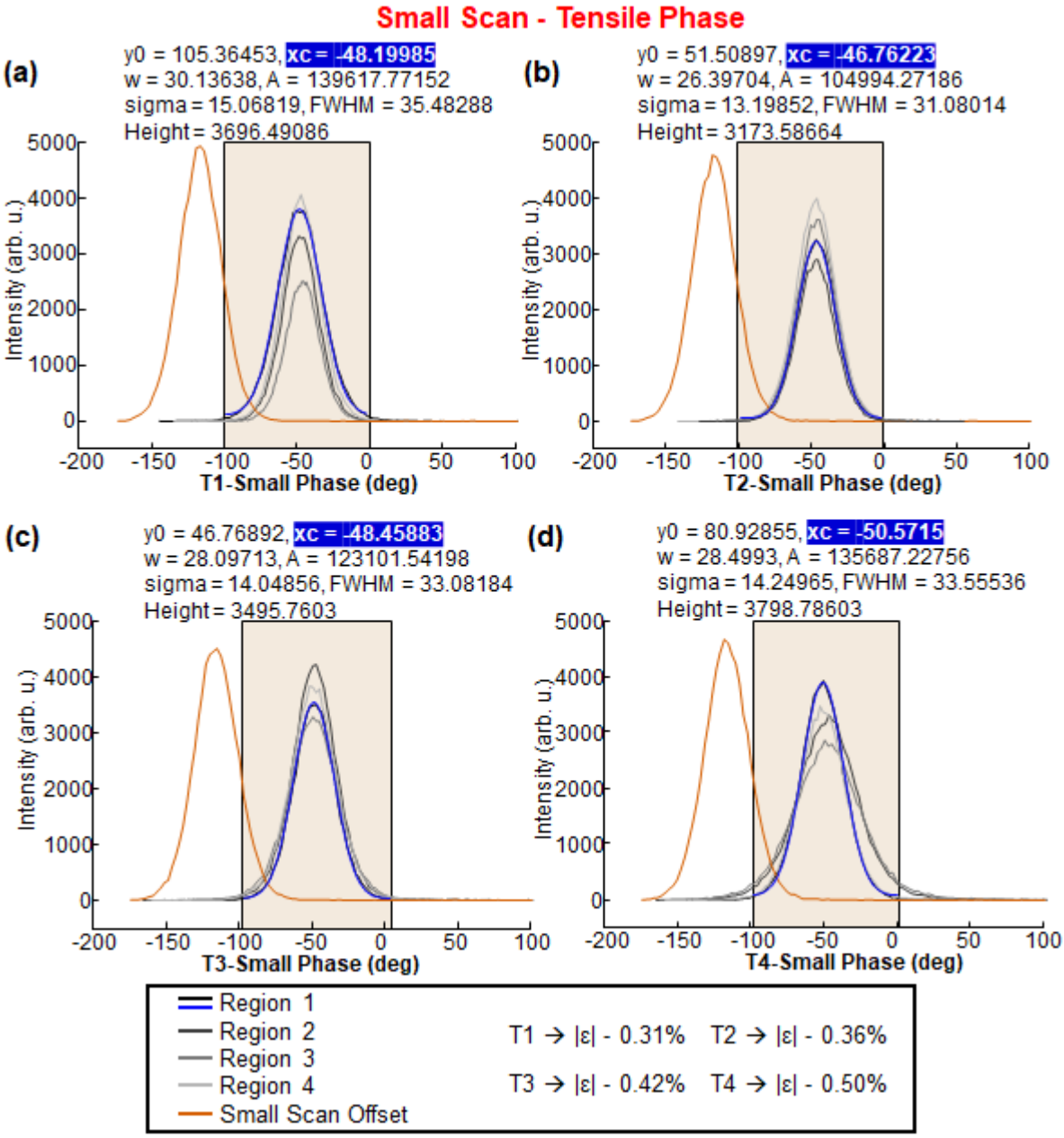

Figure S17. Small scan area PFM Phase image intensity distributions of selected regions on ZnO-NS surface for tensile regime at an absolute strain of (a) 0.31%, (b) 0.36%, (c) 0.42%, and (d) 0.50%. Extracted mean for single selected small scan region ZnO-NS phase response highlighted in blue.